# Decay of eddies at the South-West Indian Ridge

**Authors:**
Jonathan V. Durgadoo[1,2]
Isabelle J. Ansorge[1]
Beverly A. de Cuevas[3]
Johann R.E. Lutjeharms[1]
Andrew C. Coward[3]

**Affiliations:**
[1]Department of Oceanography, University of Cape Town, Cape Town, South Africa

[2]Leibniz-Institut für Meereswissenschaften (IFM-GEOMAR), Kiel, Germany

[3]Marine Systems Modelling Group, National Oceanography Centre, University of Southampton, Waterfront Campus, Southampton, United Kingdom

**Correspondence to:**
Jonathan Durgadoo

**Email:**
jdurgadoo@gmail.com

**Postal address:**
Private Bag X3, Rondebosch 7701, South Africa

**Dates:**
Received: 25 Mar. 2011
Accepted: 23 June 2011
Published: 03 Nov. 2011

**How to cite this article:**
Durgadoo JV, Ansorge IJ, De Cuevas BA, Lutjeharms JRE, Coward AC. Decay of eddies at the South-West Indian Ridge. S Afr J Sci. 2011;107(11/12), Art. #673, 10 pages. http://dx.doi.org/10.4102/sajs.v107i11/12.673



The South-West Indian Ridge in the Indian sector of the Southern Ocean is a region recognised for the creation of particularly intense eddy disturbances in the mean flow of the Antarctic Circumpolar Current. Eddies formed at this ridge have been extensively studied over the past decade using hydrographic, satellite, drifter and float data and it is hypothesised that they could provide a vehicle for localised meridional heat and salt exchange. The effectiveness of this process is dependent on the rate of decay of the eddies. However, in order to investigate eddy decay, logistically difficult hydrographic monitoring is required. This study presents the decay of cold eddies at the South-West Indian Ridge, using outputs from a high-resolution ocean model. The model's representation of the dynamic nature of this region is fully characteristic of observations. On average, 3–4 intense and well-defined cold eddies are generated per year; these eddies have mean longevities of 5.0±2.2 months with average advection speeds of 5±2 km/day. Most simulated eddies reach their peak intensity within 1.5–2.5 months after genesis and have depths of 2000 m – 3000 m. Thereafter they dissipate within approximately 3 months. The decay of eddies is generally characterised by a decrease in their sea surface height signature, a weakening in their rotation rates and a modification in their temperature–salinity characteristics. Subantarctic top predators are suspected to forage preferentially along the edges of eddies. The process of eddy dissipation may thus influence their feeding behaviour.

## Introduction

Regions of high mesoscale variability in the Southern Ocean correlate closely with places where the core of the Antarctic Circumpolar Current (ACC) interacts with prominent bottom topography such as the Crozet and Kerguelen Plateaus.[1,2] Altimetric and hydrographic data[1,2] have been used to identify an additional region of high variability in the vicinity of the South-West Indian Ridge (SWIR). Hydrographic data collected during the SWINDEX (South-West Indian Ocean Experiment) surveys in 1993 and 1995 have shown that close to the SWIR the ACC splits into several branches,[3] resulting in enhanced eddy generation in the lee of the ridge. This region of high variability – characterised by an extensive train of meanders and eddies – extends eastwards from 30°E towards the Prince Edward Islands at 37°E (Figure 1). The funnelling of the greater part of the ACC through a prominent fracture in the SWIR in this region is the main cause for the generation of several branches within each frontal band as well as cyclonic and anti-cyclonic eddies.[2,4]

The DEIMEC (Dynamics of Eddy Impact on Marion's Ecosystem) programme[4] provided a set of direct measurements of eddies at the SWIR. In particular, DEIMEC IV allowed detailed hydrographic and biological characterisation of a single intense and coherent cold eddy at the ridge[5,6,7] (Figure 2). Figure 2a shows vertical sections of potential temperature and salinity across the DEIMEC IV eddy and Figure 2b presents a pair of potential temperature–salinity ($\theta$–$S$) profiles emphasising the difference in water masses associated within the core of this eddy in contrast to those found in its immediate surroundings at the time of the survey. Figure 2c, showing the trajectory of the DEIMEC IV eddy from its inception until it passed the Prince Edward Islands, provides very little information on the temporal decay of that specific feature. Whilst the descriptive characteristics and importance of such eddies at the Prince Edward Islands are relatively well understood,[5,6,7] it remains unclear, to date, how the physical attributes of intense eddies are modified over time (particularly over the full depth range). The decay of anomalies at the ridge has only been inferred from altimetric observations using the anomalous sea surface height signature to track the gradual dissipation of these eddies over time[2,8] (Figure 2c). The effect that dissipation has over time on the subsurface structure of eddies at the ridge also remains unknown. It is anticipated that a few mechanisms contribute to the gradual erosion of a mesoscale eddy. It is assumed that the upper layer is subjected to active air–sea exchanges, promoting the weakening of its surface temperature and salinity signatures.[9] Lateral exchange of properties with

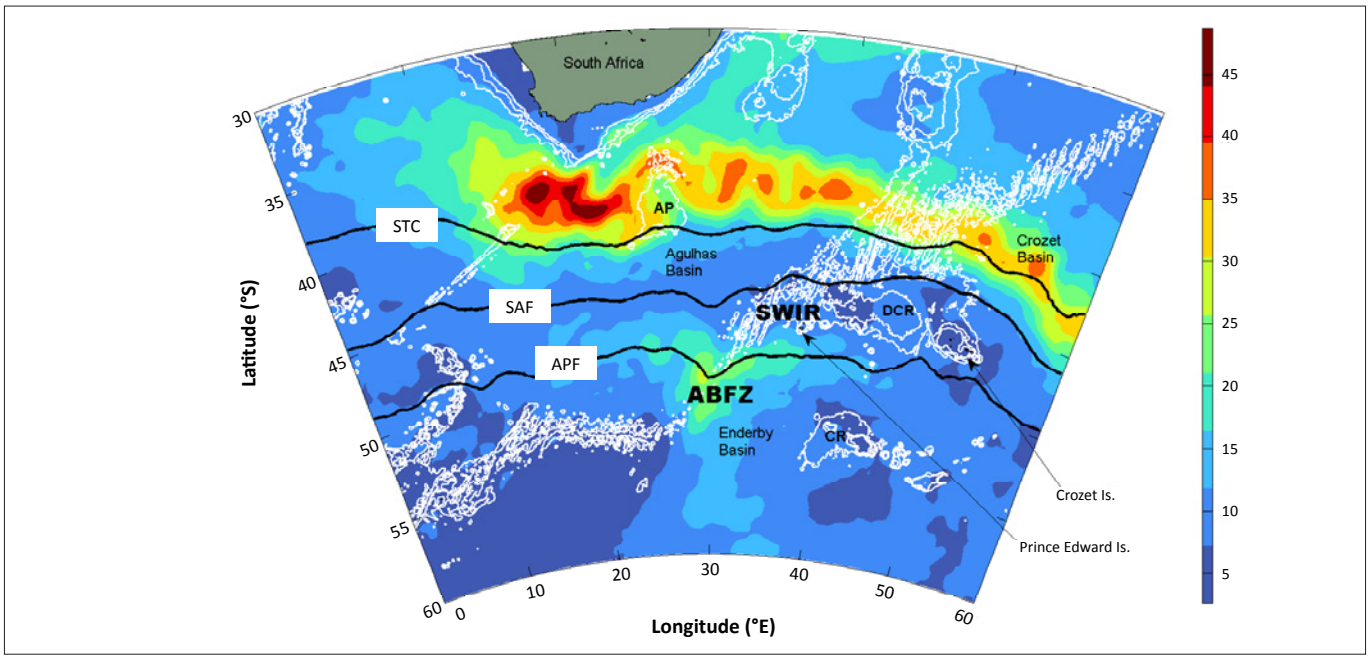


*Source*: Durgadoo et al.[4]

**FIGURE 1:** The root-mean-square sea surface height (cm) calculated from a 13-year record of altimetry products. Bathymetric contours (–3000 m, –2000 m, –1000 m) are overlaid in white. The average positions of the three major fronts associated with the Antarctic Circumpolar Current are shown: the Subtropical Convergence (STC), the Subantarctic Front (SAF) and the Antarctic Polar Front (APF). Some important topographic features are also shown: the South-West Indian Ridge (SWIR), the Andrew Bain Fracture Zone (ABFZ), the Conrad Rise (CR), the Agulhas Plateau (AP) and the Del Cano Rise (DCR).

the surrounding environment, usually by means of double-diffusion and interleaving, leads to the further dissipation of the anomalous heat and salt content of a feature. These mechanisms may also have a seasonal variation. In addition, the merging or splitting of a feature enhances or lowers its anomalous sea surface height signature. Local bottom topography ought to further influence the intensity and trajectory of a feature.[9]

The advent of improved high-resolution ocean model platforms has facilitated the ease in which the study and analysis of mesoscale features over time can be achieved, particularly in parts of the ocean otherwise difficult to reach. Using outputs from an appropriate numerical model to study eddies at the SWIR provides a potentially useful way to examine and follow their decay and water mass transformation. In this study we used the Ocean Circulation and Climate Advanced Modelling $\frac{1}{12}^{\circ}$ model output to identify, track and describe the decay of cold eddies at the SWIR. The nominal horizontal and vertical resolution of this model makes it suitable for such a study.

## The Ocean Circulation and Climate Advanced Modelling model

The Ocean Circulation and Climate Advanced Modelling (OCCAM) model was adapted from the Modular Ocean Model[10] with various improvements made by the OCCAM group. The rigid-lid was replaced with a free-surface scheme that uses a tidal model to resolve the barotropic equations and the modified split-QUICK advection scheme was introduced.[11] The K-Profile Parameterisation vertical mixing scheme proposed by Large et al.[12] was adopted. The arrangement of variables in the horizontal follows the Arakawa-B grid and a scaled coordinate is used in the vertical with 66 levels, giving a better representation of the mix-layer dynamics. Detailed documentation on the set-up of the model is provided by Coward and de Cuevas.[13]

The model tracer fields were initialised using the World Ocean Circulation Experiment Special Analysis Centre climatology, the World Ocean Atlas and the Arctic Ocean Atlas data.[13] Surface forcing is achieved using a bulk layer formulation for heat and momentum, eliminating the need for surface potential temperature relaxation. Atmospheric fields such as: (1) the 10-m wind speed; (2) the 2-m air temperature and specific humidity; and (3) cloud fraction, solar radiation and precipitation have been combined with the top-level potential temperature to calculate the wind stress, the turbulent fluxes and the net long-wave radiation. The 6-hourly wind speed, air temperature and specific humidity were obtained from the National Centres for Environmental Prediction re-analysis.[14] Monthly precipitation was obtained from a combination of satellite microwave data and observations,[15,16] whilst cloud fraction and solar radiation data were obtained from the International Satellite Cloud Climatology Project data set.[17] Salinity relaxation towards the monthly Levitus et al. data fields[18] was used over the upper 20 m with a 45-day timescale in an attempt to ensure that the lack of explicit run-off and any deficiencies in the precipitation fields were accounted for. For this study, we used 5-day-mean data from the hind-cast run 401 ($\frac{1}{12}^{\circ}$ horizontal resolution with 66 vertical levels) for the years from 1989 to 1998 (inclusive).

### Identification and tracking of eddies

Relatively straightforward identification and tracking of eddies has been made possible by looking at sea surface

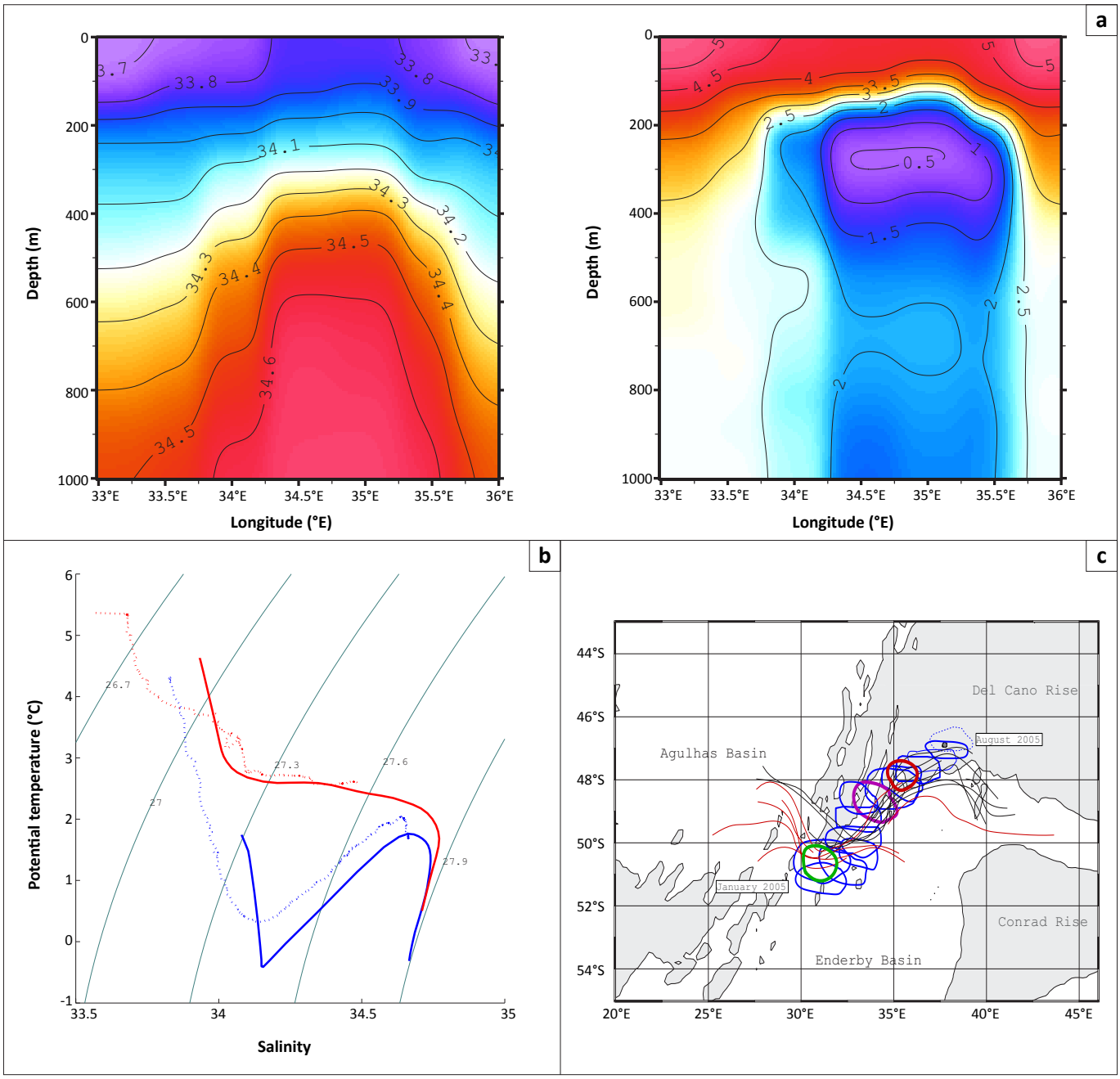


*Sources*: DEIMEC plots were adapted from Ansorge et al.[5] and Swart et al.[7] Altimetry data trajectories were obtained from Ansorge and Lutjeharms[2].

**FIGURE 2:** (a) Zonal sections of salinity (left) and potential temperature (°C, right) across a cold eddy at the South-West Indian Ridge obtained by the Dynamics of Eddy Impact on Marion's Ecosystem (DEIMEC) IV. (b) Two pairs of θ–*S* plots within (blue) and outside (red) of the eddy shown in Figure 3 (solid lines) and the DEIMEC IV eddy (dotted line). Isopycnals $\sigma_{(z=0)}$ are also shown. (c) Trajectories of positive (solid black lines) and negative (red lines) sea level anomalies from altimetry. The position of the DEIMEC IV eddy over time is shown using the –20 cm sea level anomaly. Green, magenta and red circles indicate the time of inception, position at time of survey and a period of stagnation, respectively.

height anomaly (SSHA) maps, derived from an array of satellite altimeters or from numerical models. OCCAM sea surface height 5-day-mean fields were averaged over the 10-year period and the individual SSHA fields were calculated, taking into account the inverse barometer effect.

Isern-Fontanet et al.[19], adopting a general method developed by Jeong and Hussain[20], have derived a parameter, *Q*, representing the balance between shear strain rate and vorticity from a two-dimensional velocity field:

$$Q = -\left[\frac{\partial u}{\partial x}\right]^2 - \left[\frac{\partial v}{\partial x}\right]\left[\frac{\partial u}{\partial y}\right] \qquad \text{[Eqn 1]}$$

where *u* and *v* are the horizontal velocities in the *x* and *y* directions, respectively. Eddies are identified by clusters of positive *Q* values where, in an elliptic fluid flow, rotation dominates deformation. Choosing an adequate threshold for *Q* is necessary in order to capture connected entities. However, the choice of a threshold is subjective. Several choices of threshold were tested. We focused on identifying intense cold eddies, applying a *Q* threshold of 1 x $10^{-10}$/s$^2$ in conjunction with a core SSHA threshold of –30 cm, which was deemed suitable based on previous studies.[4] The position of an eddy, to one decimal place of latitude and longitude, is taken at its centre. Manual tracking of anomalies commences

when they reach a SSHA magnitude of 15 cm and ends when they decay to the same value. In so doing, weak features are filtered out.

## Model validation – Cold eddies

A snapshot section across a model cold eddy centred at 50°S, 33°E is shown in Figure 3. This particular eddy, approximately 110 km in diameter, has a strikingly distinct subsurface temperature minimum core (θ< 0 °C) at 350 m, which is capped by a well-mixed surface layer which is colder and more saline than the ambient waters. A strong halocline at 500 m marks the boundary between the temperature minimum core and deep water. Salinity distribution within the anomaly increases sharply (from 34.1 to 34.7) with depth until 1000 m below the surface. Thereafter, a thick homogenous layer of deep water ($S$ = 34.7 – 34.75) is observed between 1000 m and 2500 m. In contrast, temperature within the anomaly below 1000 m gradually decreases, but still maintains a ~0.5 °C difference with the immediate surroundings. The salient shoaling of temperature and salinity isolines is indicative of an upwelling of deeper waters, which is typical of cold eddies in the Subantarctic.[7] Full-depth velocity across this eddy shows a well-defined cyclonic rotation with velocities at the edges of the eddy exceeding 50 cm/s at the sea surface, decreasing to ~0 cm/s at the centre. The western edge of the eddy, with higher velocities, is broader and deeper than the eastern edge. This difference indicates a net eastward to north-eastward advection of the feature, which reinforces the velocities at the western edge. There is a gradual decrease of velocities with depth until ~2500 m, where the rotation at the centre is reversed. This finding indicates that, according to the model, an eddy at the SWIR can reach depths of up to 2500 m – 3000 m.

The anomalous temperature–salinity content of this modelled eddy relative to its surroundings is further highlighted in Figure 2b. The θ–$S$ profiles illustrate the distinct difference in properties at the centre of the feature from the ambient waters. The surface water within the eddy is characteristic of Antarctic Surface Water with temperatures decreasing from 1.7 °C to –0.5 °C at a quasi-uniform salinity of 34.15. Below this layer lies a temperature minimum core (θ = –0.5 °C, $S$ = 34.2) typical of Winter Water.[21] Circumpolar Deep Water is thereafter identified between 1000 m and 3000 m. The θ–$S$ properties of the ambient water are in stark contrast from those within the eddy. Surface water in the Antarctic Polar Frontal Zone, between the Subantarctic Front and the Antarctic Polar Front, consists of gradually modifying Subantarctic and Antarctic Surface Waters. Deep water in this transitional zone is marked by an increasing salinity signature from 34.4 to 34.7, at almost constant temperature of ~2.3 °C. In both profiles, a bow-shaped salinity maximum, found at $\sigma_0$ ~ 27.85, marks the location of the Lower Circumpolar Deep Water[22] and delimits the depth at which the difference in properties between the eddy and its surroundings becomes negligible. It is evident that water properties within the cold eddy are significantly different from those of the immediate surroundings. This difference is not only observed at the surface and subsurface but throughout the entire feature.

How well does the simulated eddy compare to those observed at sea? The answer to this question will allow us to estimate the verisimilitude of the model simulations. The model eddy shown in Figure 3 exemplifies an eddy of Antarctic origin within the Antarctic Polar Frontal Zone which is similar to the one surveyed during DEIMEC IV (Figure 2). There are clear similarities between the model eddy and that of DEIMEC IV. This strong agreement gives us substantial confidence that the model simulates these features well. Over 10 years, 20 such cold intense eddies were identified within the model (Figure 4). In all cases, the anomalies reached a SSHA magnitude of at least 30 cm.

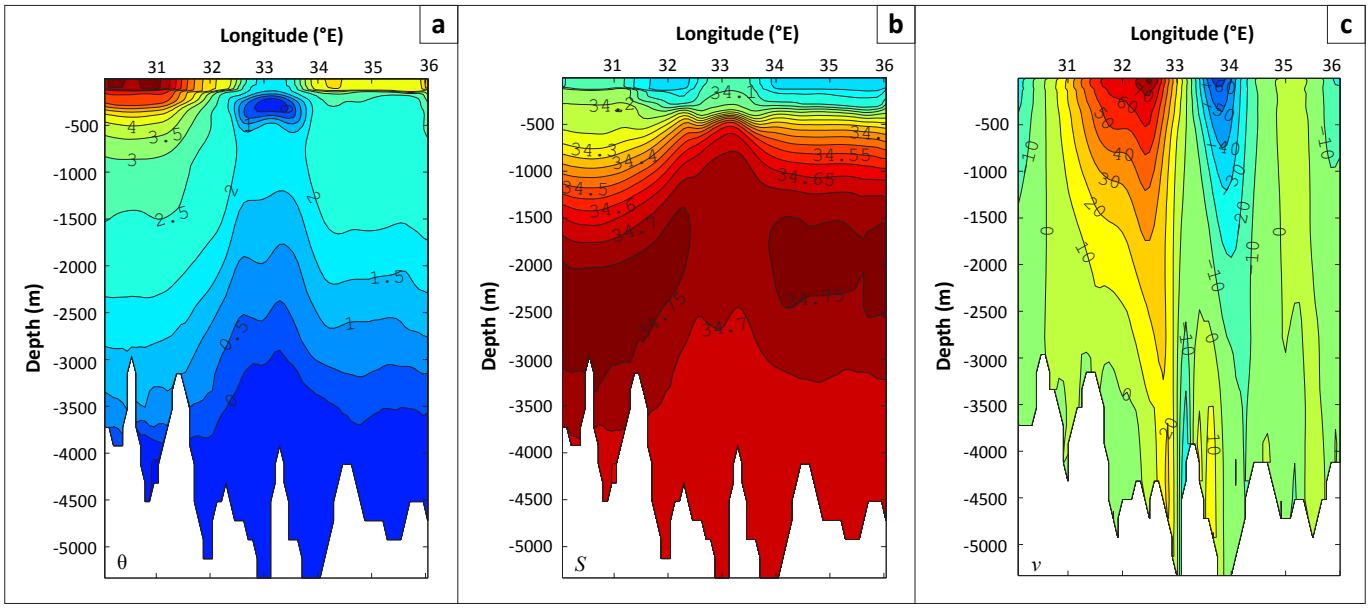


**FIGURE 3:** Full-depth zonal sections along 50°S (between 30°E and 36°E) showing the vertical structure of a simulated negative anomaly. Isolines of (a) potential temperature (θ), (b) salinity ($S$) and (c) full-depth velocity ($v$), are contoured at 0.5-°C, 0.05 and 10-cm/s intervals, respectively. The blank portions indicate the local bathymetry.

The trajectories of the 20 intense modelled eddies show some degree of coherence and the general pattern agrees well with altimetric observations (Figure 2c). The eddies were generated immediately east of the Andrew Bain Fracture Zone (30°E – 33°E) and they travelled in a north-easterly direction following the eastern flank of the ridge until 37°E. Thereafter, they drifted eastward, where some meandering in their paths is also observed. Between 32°E and 37°E, the eddies closely followed the $f/h$ = 0.4 rad/s.m contour. Thereafter, the strong topographic control on the trajectories seems to be lost. The mean trajectory of the eddies beyond 34°E is mostly eastward. Two zonal time–longitude plots, along 48.5°S and 48°S (between 30°E and 45°E), depicted in Figure 5 show the propagation of anomalies having SSHA < –15 cm. It is important to note that the threshold for the parameter $Q$ has been relaxed to $Q > 0/s^2$ to account for the meandering advection of some eddies. Several clear conclusions can be made about eddies spawned at the ridge. The temporal record shows few long-lived features (> 7 months) and some features seem to be stagnant for at least 4–6 months. An average of 3–4 anomalies per year are simulated between 33°E and 40°E by the model and very few features are present east of 43°E, consistent with previous results.[23] Furthermore, an increased advection speed is noted along 48°S. On average, the simulated mesoscale eddies are short-lived, have longevities of only 5.03±2.23 months and travel at a speed of 5.49±1.59 km/day over a distance of 785±310 km. These values are reasonably commensurate with direct hydrographical observations at the ridge following the DEIMEC cruises.[4] Morrow et al.[24] have pointed out that features shed meridionally across zonal currents, like the ACC, tend to be quickly re-absorbed into the mean flow.

## Decay of eddies

In Figure 4, most of the simulated eddies have spun down before reaching 39°E. Only three features are observed to be travelling east beyond 41°E. The longitudinal evolution in SSHA signal of the features is presented in Figure 6a. Soon after inception between 31°E and 33°E, the simulated eddies have the largest variability in SSHA. More than 75% of the features are observed to have travelled between 32°E and 37°E. A peak in mean SSHA value (~40 cm) between 39°E and 40°E is noted, but with the decreasing number of observations available beyond 38°E, this local maximum may not be significant. Complementing the above, the change in SSHA of the 20 features with time is shown in Figure 6b. It is obvious that each individual eddy is distinctly different. On average, the initial generation period is approximately 1–2 months. During that time, an eddy evolves into a fully fledged, isolated feature with an overall increasing SSHA signature. A broad range of maximum intensities is noted and most eddies reach their peak intensity between 30 and 90 days after genesis. Most features undergo a decay period of about 3 months which is characterised by a gradual decrease in their SSHA signature.

We have focused on two disparate cold eddies and describe the change with age in some of their physical properties: their simulated SSHA signature, full-depth velocity and anomalous temperature and salinity. Figures 7 and 8 present case studies of these two eddies tracked within the model. Zonal sections of potential temperature, salinity and meridional velocity across each eddy at three different stages (Locations A, B and C) of their lifetimes are shown. Tracking started at Location A and ended at Location C, where the eddy could no longer be unambiguously identified using the combination SSHA < –15 cm and $Q > 1 \times 10^{-10}/s^2$. Location B was taken during mid-life. In addition, a θ–$S$ plot, showing the change in the water mass at the core of the feature, and the complete track extracted from Figure 4, are shown.

Eddy 1 (Figure 7) was the longest-lasting feature (300 days or 10 months; April – February) and travelled the greatest distance (1422 km) amongst the collection of 20 eddies. Its

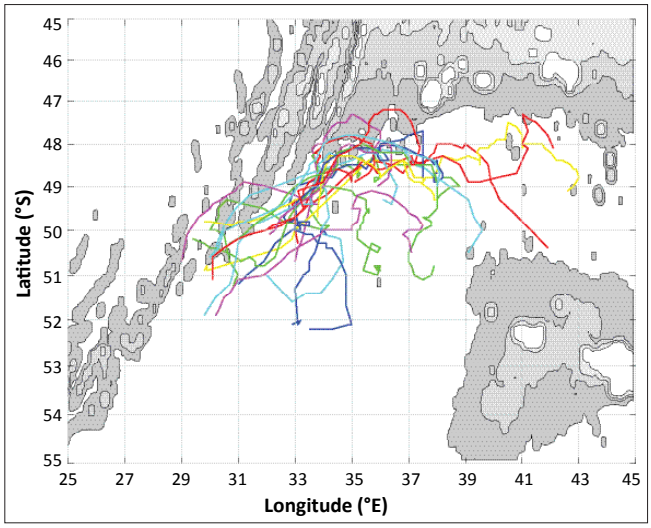


**FIGURE 4:** Trajectories of 20 negative anomalies tracked in the 10-year Ocean Circulation and Climate Advanced Modelling data set. The magnitude of the $f/h$ contours (0.1 rad/s.m – 0.4 rad/s.m) are shown at 0.1-rad/s.m intervals.

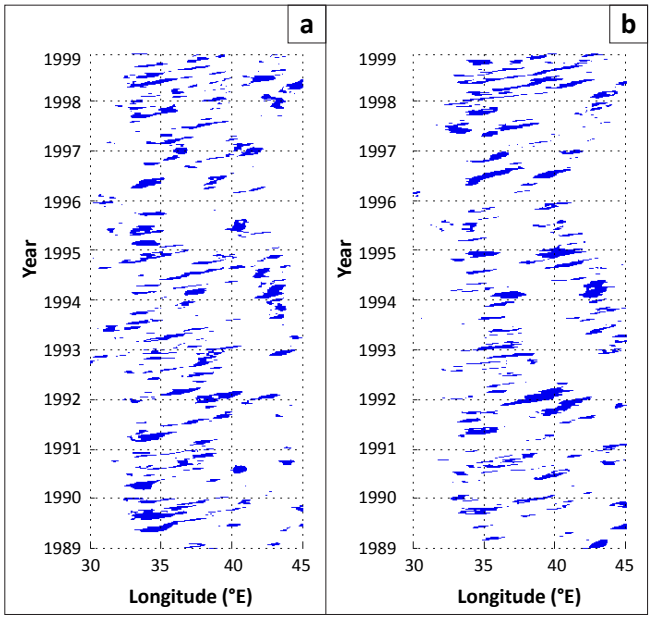


**FIGURE 5:** Temporal Hovmöller plots along (a) 48.5°S and (b) 48°S showing the propagation of negative anomalies using the sea surface height anomaly, SSHA < –15 cm and $Q > 0/s^2$ criteria.

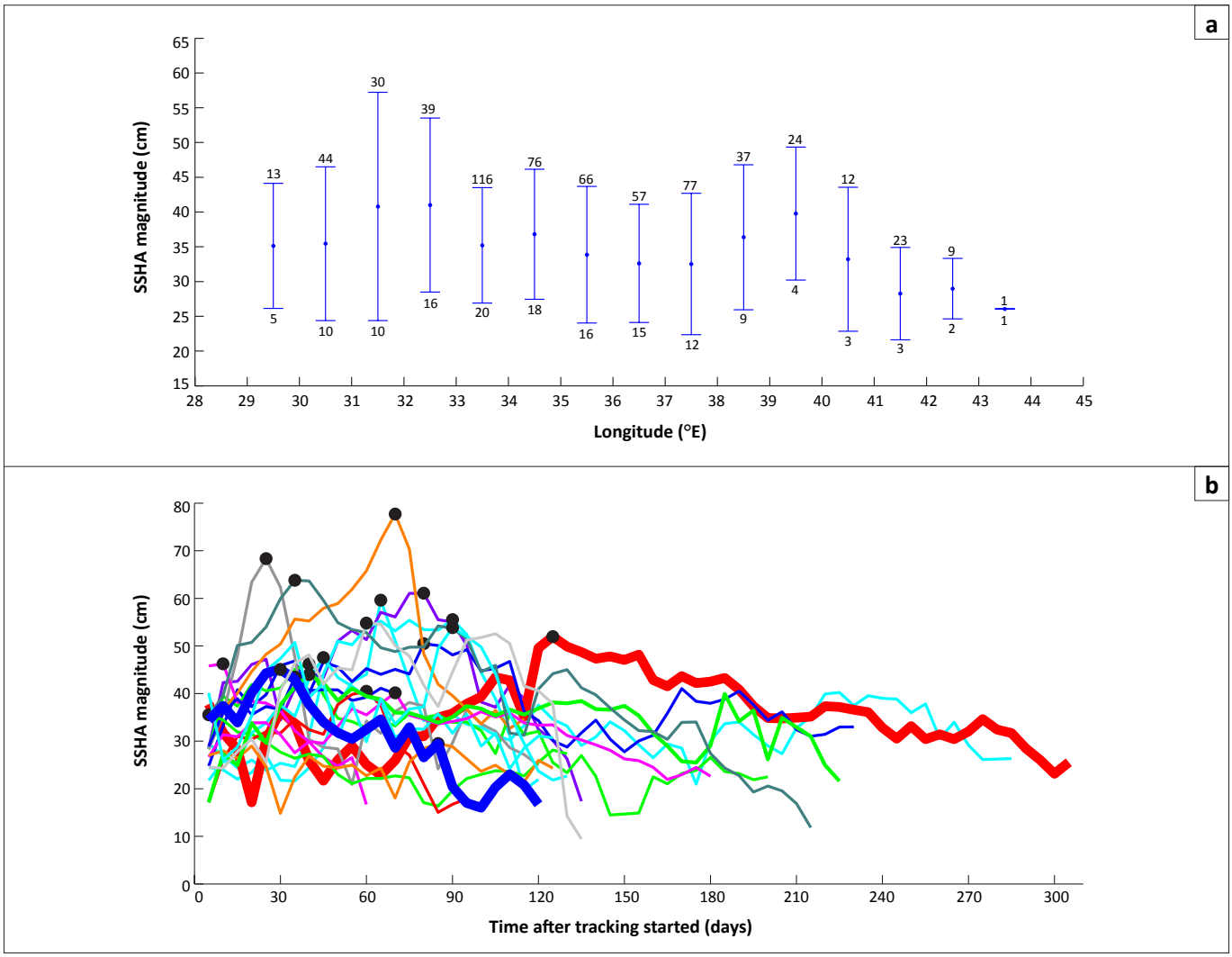


**FIGURE 6:** The decay in sea surface height anomaly (SSHA, magnitude in cm) of 20 simulated cold eddies tracked at the South-West Indian Ridge. (a) Mean ± standard deviation of SSHA showing decay with longitude. The values above the error bars indicate the number of observations used to calculate the mean ± standard deviation per degree longitude, whilst those below the error bar indicate the number of cold eddies (out of 20) reaching that longitude. (b) The temporal evolution of SSHA – dots indicate the time after generation at which each eddy reached its maximum intensity. The evolutions of two eddies are highlighted using thick lines: Eddy 1 is shown in red and Eddy 2 is shown in blue.

average propagation speed of 4.74 km/day was below the overall mean. The distance covered by Eddy 1 between Locations A and B was 968 km, which is almost twice as much as the distance between Locations B and C, over the same period of 5 months (150 model days). This particular eddy reached its maximum intensity 4 months after generation (Figure 6b) and remained at about that level of intensity (~–47 cm) for about a month. In this case, maturity occurred in a region where other eddies usually dissipate, between 38°E and 40°E. Uncharacteristically, it took a longer time to decay, lingering between the Del Caño and Conrad Rises. The $\theta$–$S$ profiles at the core of the eddy unmistakably characterise this eddy as being of Antarctic origin. However, it is surprising that the eddy underwent only a slight modification in water mass structure despite the distance covered and its slow translation. Close inspection of the vertical sections revealed some useful information. At the generation stage, Eddy 1 was recognisable by the shallow (~200 m) and wide (~175 km in diameter) layer of temperature minimum core and shoaling temperature and salinity isolines. The velocity structure showed a weak cyclonic rotation, which was slightly stronger and more defined at its western edge. At maturity the eddy reached a depth of about 2000 m – 3000 m and the rotation was recognisable. Furthermore, the surface and subsurface expressions of the eddy were also very distinct from those of the surrounding waters. At its final stage (position C), where tracking was terminated, the surface expression of the feature was homogenised to such an extent as to make it difficult to be identified from its SST and SSHA signatures. It is evident, however, that remnants of the eddy were still present.

In contrast to the first eddy, Eddy 2 (Figure 8) was short-lived, lasting only 115 days (October – January). Its translation speed of 7.06 km/day was, however, well above average and, as a result, it travelled a distance of 812 km. This particular eddy closely followed the $f/h$ = 0.4 rad/s.m contour of the eastern flank of the SWIR between Locations A and B. It rapidly reached its peak intensity 1 month after generation, and thereafter decayed gradually (Figure 6b). At Location A, it is evident from the velocity section that the feature

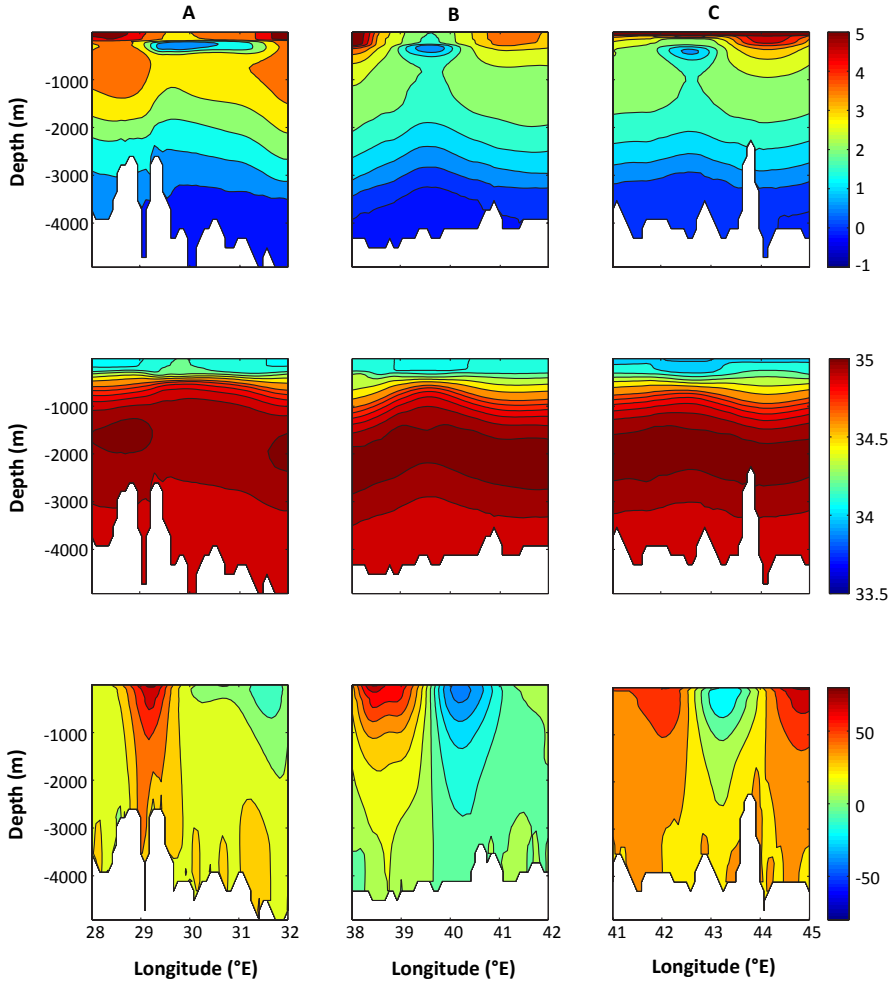


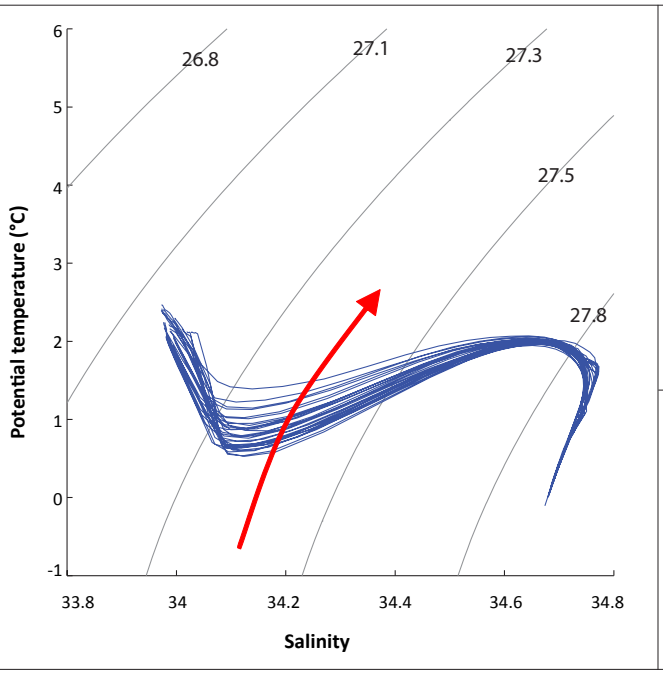


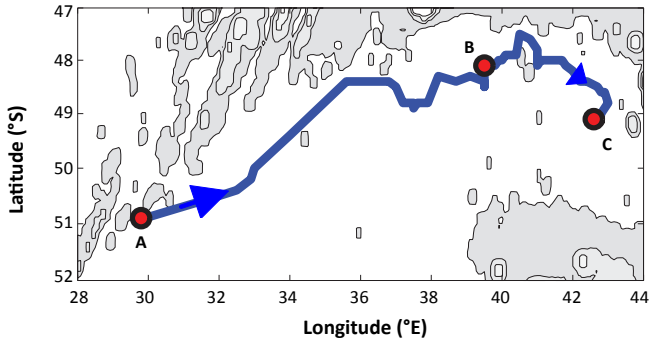


| Locations | Model day | Latitude (°S) | Longitude (°E) |
|---|---|---|---|
| A | 2300 | 50.9 | 29.8 |
| B | 2450 | 48.1 | 39.5 |
| C | 2600 | 49.1 | 42.6 |

**FIGURE 7:** Full-depth zonal sections across Eddy 1 at three locations (A, B and C), corresponding to where tracking started, during mid-life and when tracking ended, respectively. The top panel shows the potential temperature sections (contours at 0.5-°C intervals); the middle panel shows the salinity sections (contours at 0.1 intervals between 33.5 and 34.5 and at 0.05 intervals between 34.5 and 35); and the bottom panel shows the meridional full-depth velocity $v$ (contours at 10-cm/s intervals). The $\theta$–$S$ plot shows the decay in water mass – one profile taken at each time step at the core of the eddy. The track of Eddy 1 is also shown – the plot is similar to that shown in Figure 4. Arrows indicate the timeline from A to C.

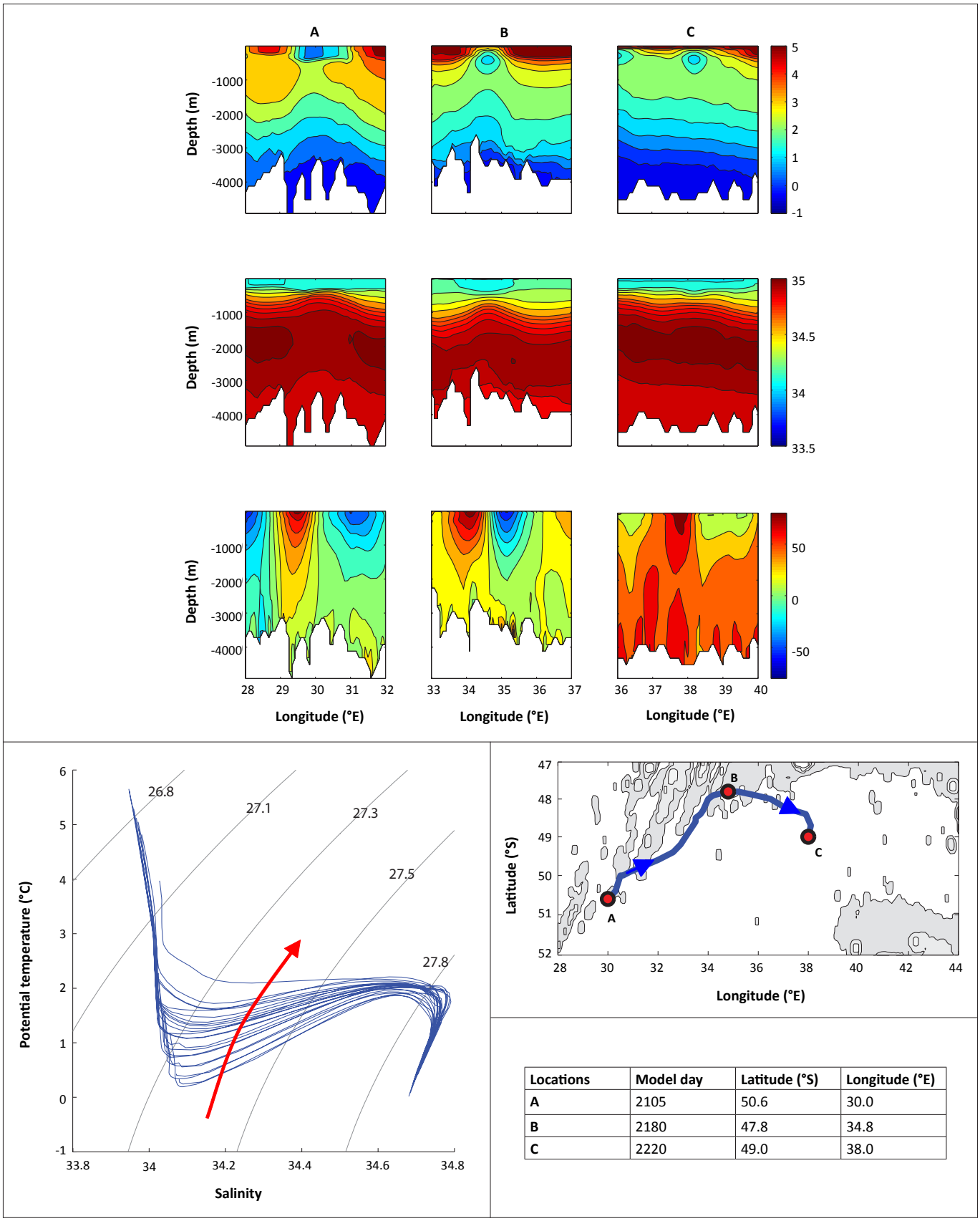


| Locations | Model day | Latitude (°S) | Longitude (°E) |
|---|---|---|---|
| A | 2105 | 50.6 | 30.0 |
| B | 2180 | 47.8 | 34.8 |
| C | 2220 | 49.0 | 38.0 |

**FIGURE 8:** Full-depth zonal sections across Eddy 2 at three locations (A, B and C), corresponding to where tracking started, during mid-life and when tracking ended, respectively. The top panel shows the potential temperature sections (contours at 0.5-°C intervals); the middle panel shows the salinity sections (contours at 0.1 intervals between 33.5 and 34.5 and at 0.05 intervals between 34.5 and 35); and the bottom panel shows the meridional full-depth velocity $v$ (contours at 10-cm/s intervals). The $\theta$–$S$ plot shows the decay in water mass – one profile taken at each time step at the core of the eddy. The track of Eddy 2 is also shown – the plot is similar to that shown in Figure 4. Arrows indicate the timeline from A to C.

was not at the initial stage of development. In this case, the selection fields used to identify eddies failed to capture this feature at its true inception. Water masses at the core of this eddy showed significant modification throughout the water column, with a pronounced change in potential temperature of ~2 °C along the $\sigma_0 = 27.3$ isopycnal. At Location C, the eddy had decayed almost completely. The remnant of the feature could only be identified in the potential temperature section with a central subsurface minimum between ~200 m and ~600 m. The isotherms, as well as the isohalines, below that level showed relatively strong stratification. Furthermore, the velocity section showed that the rotation velocity dropped from >50 cm/s to ~10 cm/s.

Both eddies originated in the Antarctic Zone, at about 51°S, 30°E, with an SSHA signature of about –35 cm. However, they differed in their character, trajectory and decay, as do those observed at sea. Eddy 2 travelled at a greater speed but over a shorter distance than did Eddy 1. The peak intensity reached by both eddies was comparable. It took 4 months (40% of its life) for Eddy 1 to reach its peak intensity. Thereafter, Eddy 1 underwent a slow and gradual decrease in SSHA signature. In contrast, Eddy 2 took only 1 month (25% of its life) to evolve fully and thereafter spun down relatively fast. The trajectories taken by the eddies suggest that bathymetry may impact on the way they decayed. After generation, Eddy 1 drifted and remained in the Enderby Basin, whilst Eddy 2 travelled on shallower bathymetry for most of its life, which may have influenced its relatively rapid decay.

## Conclusions

Past investigations[25,26] have shown that the cross-frontal advection of mesoscale eddies may produce meridional heat and salt fluxes that balance much of the ocean–atmosphere exchange across the ACC. This has been further supported by recent studies[27] suggesting that cold eddies crossing over into the Subantarctic Zone may play a central role in altering the physical balance of the Southern Ocean. The process by which such eddy leakage occurs is not uniformly distributed around the Southern Ocean, but is concentrated at certain regions of prominent bathymetry, such as at the SWIR. In 2005, the DEIMEC IV hydrographic survey carried out the first detailed survey of a cold eddy downstream of the SWIR. Although a detailed physical and biological description of this eddy has been published,[5,6,7] the influence that such an eddy may have had on the meridional exchange of water masses, as well as the manner in which this feature decayed with time downstream of its source region, needed to be further addressed. Unfortunately, suitable observational coverage of eddies in space and time is severely limited by the difficulty of sampling using conventional shipborne instruments. In this study, we used a 10-year hindcast model data set from OCCAM $\frac{1}{12}$°. We demonstrated that this model simulates these eddies particularly well, allowing one to ask questions of the model that cannot be observed in nature. Of the 20 cold eddies tracked within the model, each individual eddy was manifestly different; these differences were supported by observations. Nevertheless, there were also some similarities in their overall behaviour. Their trajectories generally followed the eastern flank of the SWIR, in an area between 48°S – 50°S and 33°E – 37°E. Intense eddies at the SWIR lasted on average 4 months (65% of eddies tracked) and were very rapidly reabsorbed into the mean flow. Very few eddies that persisted for more than 7 months were observed. Intense cold eddies were defined as SSHA < –30 cm. The time from generation to maximum intensity varied greatly amongst individual eddies. The decay of two eddies was studied in detail. The degree of water mass decay (mixing) was ostensibly linked to the advection speed of the features. In both cases, the cyclonic rotation associated with the features also considerably weakened over distance. However, the subsurface temperature minimum core seemed to linger longer. The Prince Edward Islands host a number of top predators whose foraging behaviour is hypothesised to be linked to the passing of eddies.[28] To what extent these observed foraging patterns depend on and change as eddies dissipate over space and time is not known. It is anticipated that a correlation between the foraging behaviour of the animals and the decay of eddies exists as a result of the decreased availability of food. However, such investigations are yet to be undertaken in this region.

## Acknowledgements

We thank the South African National Antarctic Programme and the University of Cape Town for funding. Model data were acquired during a short visit to the National Oceanographic Centre, Southampton.

This manuscript is dedicated to Prof. Emeritus Johann R.E. Lutjeharms who passed away on 08 June 2011; Mentor, without whom this study would not have been possible.

### Competing interests

We declare that we have no financial or personal relationships which may have inappropriately influenced us in writing this article.

### Authors' contributions

The study was conceived by J.V.D., I.J.A. and J.R.E.L. B.A.C. and A.C.C. assisted with the model data extraction and analysis. The manuscript was put together by J.V.D. with contributions from all other authors.

## References

1. Froneman PW, Ansorge IJ, Vumazonke L, et al. Physical and biological variability in the Antarctic Polar Frontal Zone: Report on research cruise 103 of the MV SA *Agulhas*. S Afr J Sci. 2002;98:534–536.
2. Ansorge IJ, Lutjeharms JRE. Eddies originating at the South-West Indian Ridge. J Mar Syst. 2003;39:1–18. http://dx.doi.org/10.1016/S0924-7963(02)00243-9
3. Pollard RT, Read JF. Circulation pathways and transports of the Southern Ocean in the vicinity of the Southwest Indian Ridge. J Geophys Res. 2001;106:2881–2898. http://dx.doi.org/10.1029/2000JC900090
4. Durgadoo JV, Ansorge IJ, Lutjeharms JRE. Oceanographic observations of eddies impacting the Prince Edward Islands, South Africa. Antarc Sci. 2010;22:211–219. http://dx.doi.org/10.1017/S0954102010000088

5. Ansorge IJ, Lutjeharms JRE, Swart NC, Durgadoo JV. Observational evidence for a cross frontal heat pump in the Southern Ocean. Geophys Res Lett. 2006;33:L19601. http://dx.doi.org/10.1029/2006GL026174
6. Bernard ATF, Ansorge IJ, Froneman PW, Lutjeharms JRE, Bernard KS, Swart NC. Entrainment of Antarctic euphausiids across the Antarctic Polar Front by a cold eddy. Deep Sea Res I. 2007;54:1841–1851. http://dx.doi.org/10.1016/j.dsr.2007.06.007
7. Swart NC, Ansorge IJ, Lutjeharms JRE. Detailed characterisation of an Antarctic eddy in the subantarctic. J Geophys Res. 2008;113:C01009. http://dx.doi.org/10.1029/2007JC004190
8. Ansorge IJ, Lutjeharms JRE. Twenty-five years of physical oceanographic research at the Prince Edward Islands. S Afr J Sci. 2000;96:557–565.
9. Williams RG. Modification of ocean eddies by air-sea interaction. J Geophys Res. 1988;93:15523–15533. http://dx.doi.org/10.1029/JC093iC12p15523
10. Pacanowski RC, Dixon K, Rosati A. The GFDL Modular Ocean Model user guide. No. 2. Princeton, NJ: GFDL Ocean Group; 1990.
11. Webb DJ, De Cuevas BA, Richmond CS. Improved advection schemes for ocean models. J Atmos Oceanic Technol. 1998;15:1171–1187. http://dx.doi.org/10.1175/1520-0426(1998)015<1171:IASFOM>2.0.CO;2
12. Large WG, McWilliams JC, Doney SC. Ocean vertical mixing: A review and a model with a nonlocal boundary layer parameterisation. Rev Geophys. 1994;32:363–403. http://dx.doi.org/10.1029/94RG01872
13. Coward AC, De Cuevas BA. The OCCAM 66 level model: Physics, initial conditions and external forcing. Intern Doc no. 99. Southampton: Southampton Oceanography Centre; 2005.
14. Kalnay E, Kanamitsu M, Kistler R, et al. The NCEP/NCAR reanalysis project. Bull Am Meteorol Soc. 1996;77:437–495. http://dx.doi.org/10.1175/1520-0477(1996)077<0437:TNYRP>2.0.CO;2
15. Spencer RW. Global oceanic precipitation from the MSU during 1979–91 and comparisons to other climatologies. J Clim. 1993;6:1301–1326. http://dx.doi.org/10.1175/1520-0442(1993)006<1301:GOPFTM>2.0.CO;2
16. Xie P, Arkin PA. Analyses of global monthly precipitation using gauge observations, satellite estimates and numerical model predictions. J Clim. 1996;9:840–858. http://dx.doi.org/10.1175/1520-0442(1996)009<0840:AOGMPU>2.0.CO;2
17. Rossow WB, Schiffer RA. ISCCP Cloud data products. Bull Am Meteorol Soc. 1991;72:2–20. http://dx.doi.org/10.1175/1520-0477(1991)072<0002:ICDP>2.0.CO;2
18. Levitus S, Boyer TP, Conkright ME, et al. World ocean database volume 1: Introduction. NOAA Atlas NESDIS 18. Washington, DC: US Government Printing Office; 1998.
19. Isern-Fontanet J, Garcia-Ladona E, Font J. Identification of marine eddies from altimetric maps. J Atmos Oceanic Technol. 2003;20:772–778. http://dx.doi.org/10.1175/1520-0426(2003)20<772:IOMEFA>2.0.CO;2
20. Jeong J, Hussain F, Font J. On the identification of a vortex. J Fluid Mech. 1995;285:69–94. http://dx.doi.org/10.1017/S0022112095000462
21. Park Y-H, Charriaud E, Fieux M. Thermohaline structure of the Antarctic surface water/winter water in the Indian sector of the Southern Ocean. J Mar Syst. 1998;17:5–23. http://dx.doi.org/10.1016/S0924-7963(98)00026-8
22. Whitworth T, Nowlin WD. Water masses and currents of the Southern Ocean at the Greenwich meridian. J Geophys Res. 1987;92:6462–6476. http://dx.doi.org/10.1029/JC092iC06p06462
23. Ansorge IJ, Lutjeharms JRE. Direct observations of eddy turbulence at a ridge in the Southern Ocean. Geophys Res Lett. 2005;32:L14603. http://dx.doi.org/10.1029/2005GL022588
24. Morrow R, Birol F, Griffin D, Sudre J. Divergent pathways of cyclonic and anti-cyclonic ocean eddies. Geophys Res Lett. 2004;31:L24311. http://dx.doi.org/10.1029/2004GL020974
25. Gordon AL, Taylor HW. Heat and salt balance within the cold waters of the world ocean. In: Numerical models of ocean circulation. Washington DC: National Academy of Sciences, 1975; p. 54–56.
26. De Szoeke R, Levine M. The advective flux of heat by mean geostrophic motions in the Southern Ocean. Deep Sea Res I. 1981;28:1057–1085. http://dx.doi.org/10.1016/0198-0149(81)90048-0
27. Sloyan BM, Rintoul SR. The Southern Ocean limb of the global deep overturning circulation. J Phys Oceanogr. 2001;31:143–173. http://dx.doi.org/10.1175/1520-0485(2001)031<0143:TSOLOT>2.0.CO;2
28. Nel DC, Lutjeharms JRE, Pakhomov EA, Ansorge IJ, Ryan PG, Klages NTW. Exploitation of mesoscale oceanographic features by grey-headed albatross *Thalassarche chrysostoma* in the southern Indian Ocean. Mar Ecol Prog Ser. 2001;217:15–26. http://dx.doi.org/10.3354/meps217015